PHOTONICS Research

Reconfigurable nano-kirigami metasurfaces by pneumatic pressure

Shanshan Chen,[1,†] Wei Wei,[2,†] Zhiguang Liu,[3] Xing Liu,[1] Shuai Feng,[2] Honglian Guo,[2,4] and Jiafang Li[1,3,5]

[1]Key Laboratory of Advanced Optoelectronic Quantum Architecture and Measurement (Ministry of Education), Beijing Key Laboratory of Nanophotonics & Ultrafine Optoelectronic Systems, and School of Physics, Beijing Institute of Technology, Beijing 100081, China
[2]School of Science, Minzu University of China, Beijing 100081, China
[3]Institute of Physics, Chinese Academy of Sciences, Beijing 100190, China
[4]e-mail: hlguo@muc.edu.cn
[5]e-mail: jiafangli@bit.edu.cn

Received 27 March 2020; revised 9 May 2020; accepted 10 May 2020; posted 13 May 2020 (Doc. ID 393333); published 17 June 2020

Tunable/reconfigurable metasurfaces that can actively control electromagnetic waves upon external stimuli are of great importance for practical applications of metasurfaces. Here, we demonstrate a reconfigurable nano-kirigami metasurface driven by pneumatic pressure operating in the near-infrared wavelength region. The metasurfaces consist of combined Archimedean spirals and are fabricated in a free-standing gold/silicon nitride nanofilm by employing focused ion beam (FIB) lithography. The deformable spirals are instantly transformed from two dimensional (2D) to three-dimensional (3D) by the FIB-based nano-kirigami process. The 2D–to–3D transformation induces a dramatic irreversible change of the plasmonic quadruple modes and results in significant modulation in reflection by 137%. The suspended porous nano-kirigami metasurface is further integrated with an optofluidics device, with which the optical resonance is reversibly modulated by the pneumatic pressure. This work provides a strategy for tunable/reconfigurable metasurfaces, which are useful to build a promising lab-on-a-chip platform for microfluidics, biological diagnostics, chemical sensing, and pressure monitoring.

https://doi.org/10.1364/PRJ.393333

1. INTRODUCTION

Two-dimensional (2D) metasurfaces [1–3], as one of the most striking photonics research topics in the past decade, have exhibited an unprecedented capability to manipulate electromagnetic (EM) waves within the subwavelength scale and have great potential [4–6] in areas such as flat optics [2,3,7] and meta-hologram [8–11]. Toward practical applications, there is an urgent calling for tunable/reconfigurable metasurfaces that can actively control EM waves upon external stimuli [12,13]. The challenges lie in the finding of appropriate strategies to realize tunable/reconfigurable meta-atoms at the ultrathin thickness and in the given frequency domains. In the visible and near-infrared wavelength regions, in particular, versatile attempts have been made by adopting carriers [14,15], phase-changing materials [16–18], mechanical systems [19], elastic platforms [20,21], and microfluidics [22]. For example, to achieve compact optical imaging and projection systems, optical metasurfaces have been recently integrated on microelectromechanical systems (MEMS) for dynamic beam steering [23,24] and combined with liquid crystals for phase-only transmissive spatial light modulators (SLMs) [25]. Nevertheless, the reconfiguration schemes are still limited to a few options, and the increased complexity in both design and fabrication procedures needs further improvement.

Here, we propose and demonstrate a reconfigurable nano-kirigami metasurface at the near-infrared wavelengths using pneumatic pressure. The proposed metasurfaces consist of combined Archimedean spirals fabricated in a free-standing gold/silicon nitride (Au/SiN) bilayer nanofilm by focused ion beam (FIB) lithography. The spirals are a type of deformable nano-kirigami pattern that can be instantly transformed from 2D to 3D by the FIB irradiation-induced tensile stress. Compared to the deformable spirals at terahertz frequencies [26], the 2D–to–3D transformation induces a dramatic change of the plasmonic quadruple resonances in the near-infrared wavelength region, which results in significant modulation in resonant reflection by 137%. More importantly, the optical resonances are reversibly modulated by the pneumatic pressure in an optofluidics chamber through using the suspending feature of the nano-kirigami metasurface. Such a miniaturized, stable, and deformable pneumatic design at optical wavelengths

provides, to the best of our knowledge, a novel methodology to realize tunable/reconfigurable photonic nanosystems.

2. MATERIALS AND METHODS

The schematic of the reconfigurable nano-kirigami metasurfaces is shown in Fig. 1(a), where the free-standing membrane structure is integrated onto a sealed chamber. A similar setup has been employed in a terahertz device [26], where an MEMS spiral was actively modulated by a pneumatic force. However, the employed spirals in Ref. [26] had only one leg connected to the master film, as shown in Fig. 1(b), which resulted in dramatically nonuniform deformations (as seen in the Supplementary Fig. 1 of Ref. [26]). Moreover, the reported structures were too large to operate at optical wavelengths. To meet these challenges, we employed a 2D nano-kirigami pattern [Fig. 1(c)], which is composed of combined Archimedean spirals [Fig. 1(b)]. Each simplified Archimedean spiral contains a serial of 90° arcs with different radii defined as $r(n) = (n+1)r_0$, $n = 1, 2, 3\ldots$. Here we use a simple design in Figs. 1(b) and 1(c) with $r_0 = 175$ nm, $r(1) = 350$ nm, and $r(2) = 525$ nm. Such a design has two advantages. First, the combined spirals have four legs connected to the master film and thus have enhanced stability. Second, and more importantly, the spiral size can be reduced down to wavelength scale, which is desirable for the excitation of optical resonances. In such a case, under the pneumatic pressure applied by the gas flowing into the chamber, the initial 2D spirals can be deformed into 3D geometries according to the nano-kirigami deformation principles [27,28], as illustrated in Figs. 1(c) and 1(d). Moreover, if the deformation is within the elastic deformation range, such a deformation will be reversible and can be used to dynamically modulate the optical resonances of the metasurfaces, providing a simple scheme for reconfigurable metasurfaces.

To implement the proposed scheme, numerical simulations were performed using COMSOL, a commercial finite element software. The mechanical transformations of nano-kirigami meta-atoms were obtained by adopting a bilayer stress distribution model [27] on a suspended Au/SiN bilayer film with predesigned patterns. The optical reflections were simulated under an x-polarized incidence that propagated in the negative z-axis direction. Periodic boundary conditions were applied to corresponding unit cells to realize square lattice geometry in the x–y plane.

For experimental fabrications, all the structures were prepared using the FIB-based nano-kirigami method [27,28] on self-supporting Au/SiN nanofilms. The bilayer nanofilms were prepared by coating a commercial SiN film window (bonded on silicon frame, 100 μm × 100 μm × 30 nm in mesh size, 3 × 3 meshes, Norcada Inc.) with 30 nm thick gold film by e-beam evaporation. The nano-kirigami method included a high-dose milling (>600 pC/μm) and a relative low-dose irradiation (∼10–40 pC/μm), which were implemented by employing the same FIB facility (FEI Helios 600i) in one fabrication process. For the 2D combined Archimedean spirals in a square lattice, the unit separation was designed at 1.5 μm, and the size of sample areas was chosen as 40 μm × 40 μm under the consideration of optical performance, mechanical stability, and fabrication simplicity. Another consideration is that

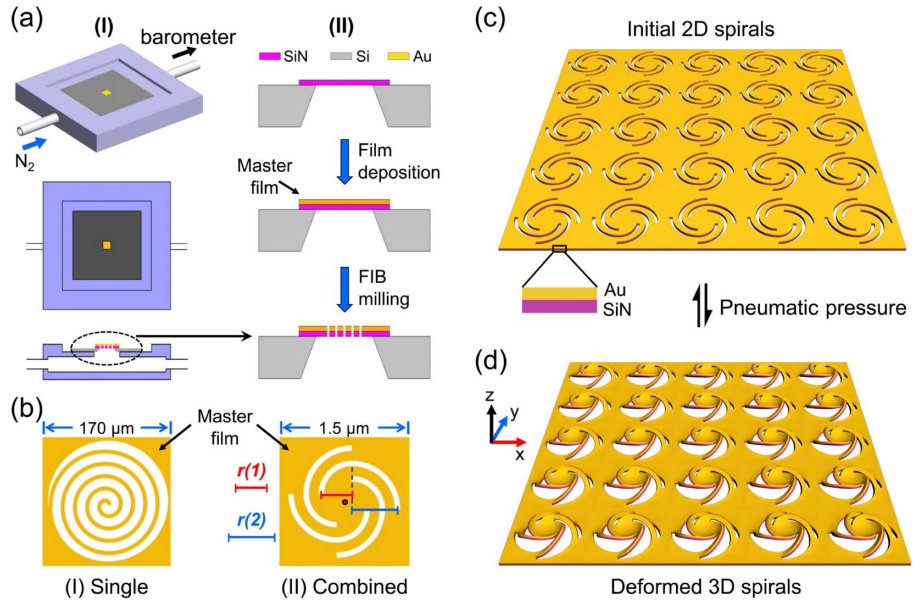

Fig. 1. (a) (I) Perspective view, top-view, and side-view schematic diagrams of a chamber for the pneumatic reconfiguration of metasurfaces (the yellow structure). One end of the chamber is inflated with nitrogen and the other end is connected to a barometer to measure the pneumatic pressure applied on the samples. (II) Schematic illustration of the fabrication process. (b) Top-view schematic of the unit cells consisting of (left) the reported single MEMS deformable spiral for terahertz polarization modulation [26], and (right) the proposed combined four Archimedean spirals in this work. Each spiral contains two 90° arcs with radius $r(1)$ and $r(2)$, respectively, and is rotated around the unit center (noted by the central red dot). The size of the combined spiral is reduced by two orders of magnitude and the stability is enhanced by its four legs connected with the master film. (c) and (d) Schematic illustrations of the proposed reconfigurable Au/SiN bilayer metasurfaces under pneumatic forces: (c) initial 2D porous spirals in a square lattice and (d) corresponding deformed 3D spirals under pneumatic pressure.

the pneumatic pressure required for reconfiguration will be dramatically increased with the reduction of the suspended structural size, although the structures could be further scaled down for operation at shorter wavelengths. The sample was finally fixed into a chamber [as illustrated in Fig. 1(a)] by applying a two-component adhesive of epoxy evenly around the nanofilms.

Optical reflection spectra were measured by using a homemade spectroscopy system. Specifically, white light from a supercontinuum light source (SC400-4, Fianium) was focused onto the samples by using a near-infrared objective lens (10×, NA 0.25, Olympus). The reflected light was collected by the same objective and delivered to a spectrometer (Ocean Optics, NIRQuest). The spectra were continuously measured during the inflation and exhaustion of nitrogen gas with an integration time of 10 ms.

3. RESULTS AND DISCUSSION

To demonstrate the proposal, the initial 2D spirals are modeled in Fig. 2(a), with $r(1) = 350$ nm and $r(2) = 525$ nm. Such a spiral structure can be deformed into 3D by applying a stress of $\sigma = 2.1$ GPa across the sample with a mechanical model [27], as shown in Fig. 2(b). The deformation not only results in an increase of the structural height along the vertical direction by $\Delta h = 130$ nm, but also induces a complex 3D twist as the outlines in Fig. 2(a). As a result, the reflection spectrum of the spirals array, initially showing a strong resonance dip at wavelength $\lambda = 2076$ nm, is shifted to 1986 nm after the 3D deformation, as shown in Figs. 2(c) and 2(d). This shift in the optical resonance results in a dramatic modification in reflection with a contrast of $\Delta R/R = 181\%$ at $\lambda = 2100$ nm ($\Delta R = R'-R$, and R and R' are the reflections of the metasurface before and after the deformation), providing an efficient way to accomplish optical reconfiguration.

To understand the mechanism behind this highly sensitive spectral shift, the electric-field (E-field) distributions of the meta-atoms before and after the deformation are plotted in Fig. 2(e). It can be seen that in the initial 2D spirals, the normalized E-field is almost completely concentrated within the gaps between the arms due to the plasmonic resonances excited at $\lambda = 2076$ nm. The mode distribution reflects the features of electric quadruple modes that are highly sensitive to the changes in structural parameters. In the case of 3D deformed spirals, the spiral plasmonic gaps are no longer uniform in width, but are twisted in 3D space. Consequently, the E-field distribution is strongly modified due to the broken symmetry, with decreased amplitude within the gaps and increased amplitude on the arms. The amplitudes of the vertical component of the E-field at the arms are also increased significantly due to the excited surface plasmons. As a result, a new resonance is excited, of which the resonant wavelength is shifted to the shorter wavelengths due to the decreased arm length in the projected x–y plane.

For experimental demonstrations, the designed 2D combined Archimedean spirals [Fig. 2(a)] are successfully fabricated using

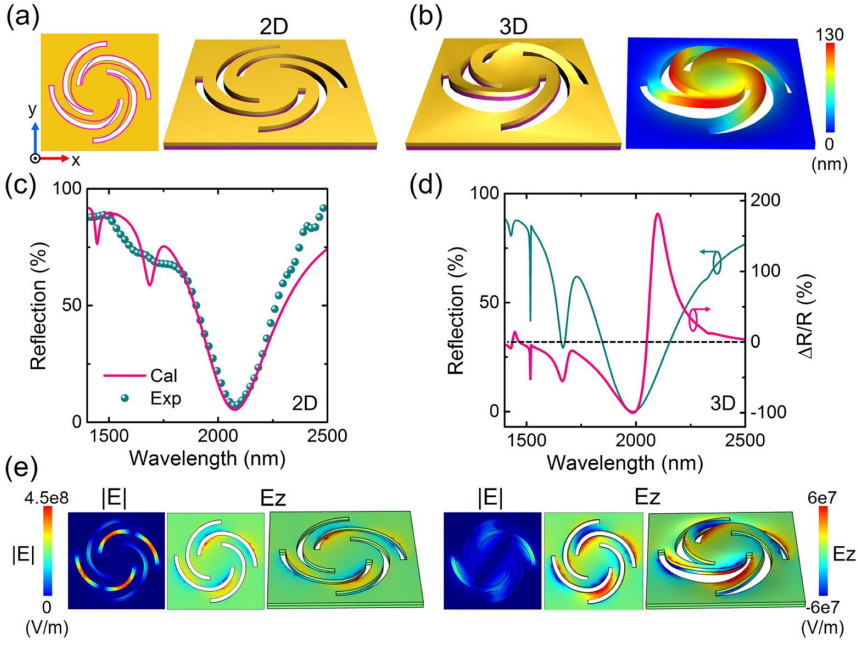

Fig. 2. (a) Schematics of the spiral unit cell and (b) the simulated 3D deformed counterpart with a deformation height of 130 nm. The violet lines in the left-side image of (a) denote the top-view outlines of the deformed spirals in (b). The right-side image of (b) shows the degree of the vertical deformation. Each spiral contains two 90° arcs with radii of 350 and 525 nm, respectively. (c) Calculated (Cal) and experimental (Exp) reflection spectra of the 2D porous metasurface. (d) (left) Calculated reflection spectrum of the deformed metasurface under a vertical deformation of 130 nm and (right) corresponding modification contrast in reflection ($\Delta R/R$) versus wavelength. The reflection spectral dip shifts from 2076 to 1986 nm with a dramatic modification of 181% at wavelength 2100 nm. (e) Top-view and side-view simulated (left) E-field distributions ($|E|$) and (right) their vertical component (E_z) for the 2D and 3D spirals at wavelength 2076 nm. The left and right scale bars correspond to the field of $|E|$ and E_z, respectively.

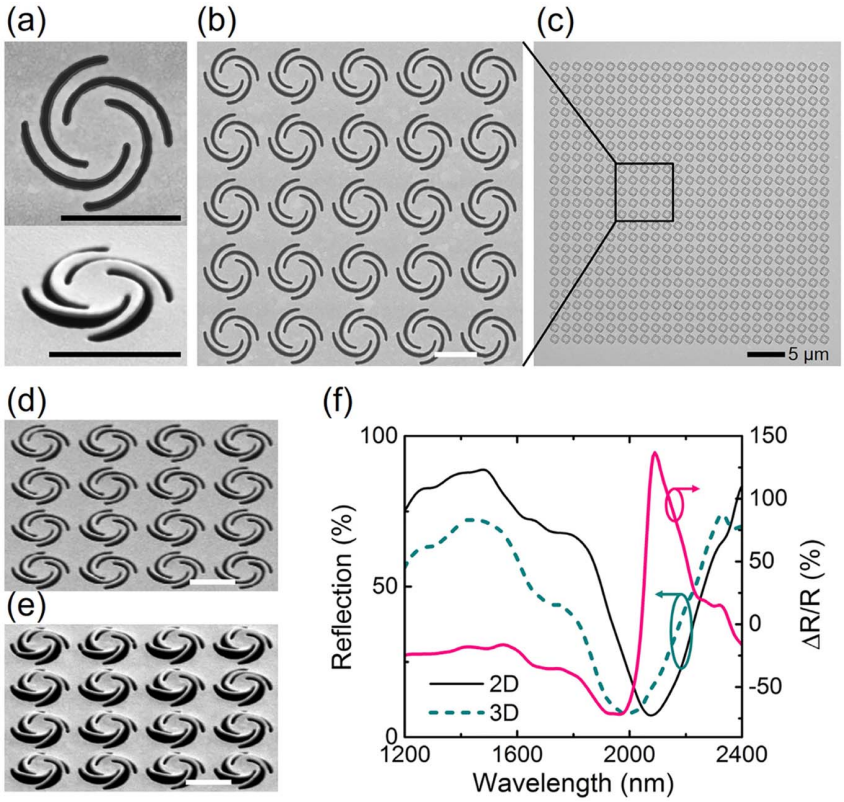

Fig. 3. (a) Top-view and side-view SEM images of a single spiral fabricated by FIB. (b) and (c) Top-view SEM images of the fabricated spirals in a square lattice. The overall size is 40 μm × 40 μm, with a periodicity of 1.5 μm. (d) and (e) Side-view SEM images of (d) 2D spirals and (e) the deformed 3D spirals by FIB-based nano-kirigami. (f) (left) Measured reflection spectra of the fabricated 2D spirals and deformed 3D spirals. (right) Corresponding modification contrast in reflection versus wavelength. The reflection spectral dip shifts from 2077 to 1989 nm with a significant modification of 137% at wavelength 2090 nm. Scale bars of (a), (b), (d), and (e) are 1 μm.

FIB, as the top-view scanning electron microscopy (SEM) images shown in Figs. 3(a)–3(c). The size of the lithographed gap is as small as ~63 nm, and the periodicity of the square lattice is 1.5 μm. The uniform array in Figs. 3(b) and 3(c) shows clearly the repeatability of the fabrication and the potential for large-scale patterning. Importantly, the experimental 2D spirals show prominent and consistent optical resonance at the main dip compared to the simulations, as shown in Fig. 2(c), which again proves the high accuracy and robustness of the FIB fabrication.

To test the deformable characteristics of the nano-kirigami patterns, the 2D spirals are instantly transformed into 3D by the same FIB through low-dose irradiation (<40 pC/μm), which induces equivalent tensile stress when grain coalescences occur around the bombardment areas of the gallium ions [27]. The side-view SEM images in Figs. 3(d) and 3(e) clearly illustrate the transformation from a 2D pattern to a twisted 3D array after the nano-kirigami process. Accordingly, the reflection spectral dip shifts from $\lambda = 2077$ to 1989 nm, with an irreversible modification of $\Delta R/R = 137\%$ at $\lambda = 2090$ nm. The consistence between calculations and experiments regarding the resonant wavelengths of 2D and 3D spirals indicates the vertically deformed height of the 3D spirals is about 130 nm. It should be mentioned that such a change is irreversible due to the elastoplastic deformation induced by FIB. Nevertheless, the observation not only proves the deformation features of the 2D spirals, but also confirms the proposal in tuning optical resonances by structural deformations, which opens up great flexibility in mechanical designs.

For the reconfiguration test, the 2D spirals sample is integrated into a microfluidics chamber, as shown by the image of the real device in Fig. 4(a). In such a configuration, the free-standing porous metasurface is fixed between two subchambers. When a certain gas or liquid is input into the subchambers with different pressures, the gas or liquid will flow through the porous metasurfaces and induce 3D vertical deformations due to the differential stress between the top and bottom surfaces. In such a way, the optical resonances from the 2D metasurface can be engineered. To test this scheme with the pneumatic force, the Port_{21} is connected to high-pressure nitrogen gas (with pressure P_2), and the Port_{22} is connected to a barometer, while subchamber #1 is open to ambient environment (with pressure P_1). When the pressure difference ($\Delta P = P_2 - P_1$) exists between subchambers #1 and #2, a differential force $\Delta F = \Delta P \cdot S$ (S is the effective area of the free-standing patterns) is introduced between the bottom and top surfaces of the structure. As a result, differential stress is induced across the sample thickness, which deforms the 2D spiral into 3D and subsequently causes a modification in the optical response. As shown in Fig. 4(c), as ΔP is tuned from 0 to 137 kPa,

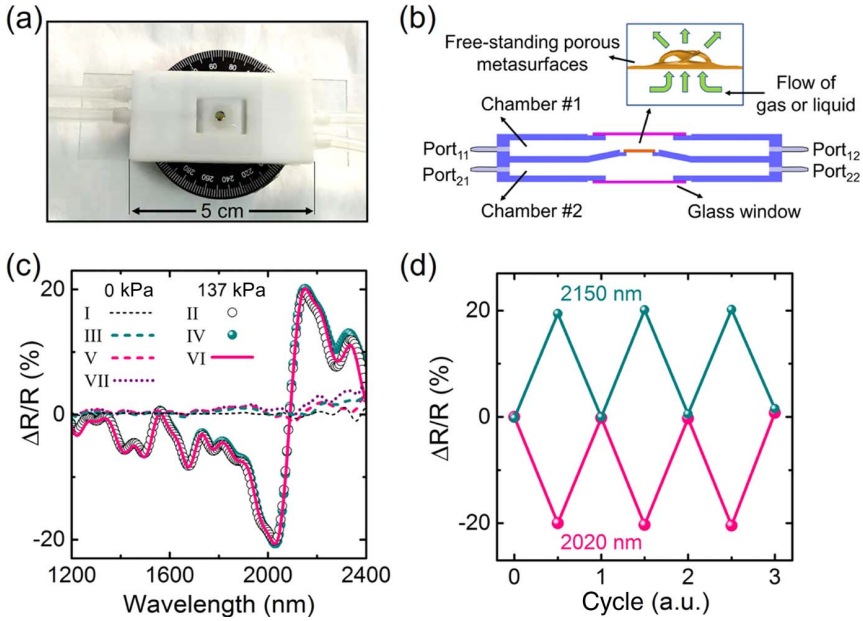

Fig. 4. (a) Camera image of the microfluidics device chamber and (b) schematic plot of the configuration for porous metasurfaces integrated in between the connect area of the two subchambers. In this configuration, when certain gas is input into the subchambers with different pressures ($\Delta P = P_2 - P_1 \neq 0$), the gas will flow through the porous metasurfaces and induce 3D deformation, which causes a change in the optical responses of the metasurfaces. (c) Measured reversible modification contrast in optical reflection from an array of four-arm spirals under repeated inflation ($\Delta P = 137$ kPa) and exhaustion ($\Delta P = 0$ kPa) of nitrogen gas. The seven curves are measured in an order of I, II, III, IV, V, VI, and VII. The high modulation under $\Delta P = 137$ kPa decreases to zero when $\Delta P = 0$ kPa. (d) Measured changes in the optical responses at two wavelengths when ΔP is tuned from 0 to 137 kPa in three cycles, showing good repeatability with a modulation contrast of ~20%.

the reflection from the metasurface is changed accordingly. Importantly, such a modification is reversible with the inflation and exhaustion of nitrogen gas; i.e., the spectral modification is repeatedly switched between $\Delta P = 137$ and 0 kPa. Specifically, the changes in the optical reflection, calculated by $\Delta R = R' - R$ (R and R' are the reflections of the metasurface without and with applied pressure), illustrate a good repeatability with a modulation contrast ($\Delta R/R$) of ~20% at two specific wavelengths, as shown in Fig. 4(d) where ΔP is tuned alternatively between 0 and 137 kPa in three cycles. Although the modulation strength in such a reversible case is smaller than that of the irreversible case [Fig. 3(f)] due to the limited pressure, it unambiguously demonstrates the potentials of reconfigurable nano-kirigami metasurfaces triggered by pneumatic pressure. It should be mentioned that the operational pressure range of this prototype structure is kept from 70 kPa to 137 kPa, where the maximum deformation ratio of the porous spirals is about 8.7%, and the repeatability is well reserved within the elastic deformation range. A further increase of ΔP (>180 kPa) may result in damage to the free-standing master film (not the porous spirals) by the high pressure due to its limited bonding strength onto the silicon frame. Therefore, further improvements of the reconfiguration performances could be made by decreasing the film thickness, optimizing the structural designs, or employing tightly bonded master film.

4. CONCLUSIONS

In summary, we have demonstrated a scheme to reconfigure near-infrared nano-kirigami metasurfaces by applying pneumatic pressure. The metasurfaces consisted of 2D combined Archimedean spirals, and the 3D deformable features were successfully tested by the FIB-based nano-kirigami process, which induced a significant modification in reflection by 137%. By using pneumatic force as the external stimulus, reconfiguration of the near-infrared optical resonances has been achieved by integrating the suspended porous metasurfaces with an optofluidics chamber, with which the optical resonances were reversibly modulated by engineering the pneumatic pressure. Our work provides what we believe, to the best of our knowledge, is a novel and simple strategy to realize tunable/reconfigurable metasurfaces, and creates a promising lab-on-a-chip platform for applications in reconfigurable optical devices, microfluidics, biological diagnostics, chemical sensing, and pressure monitoring.

Funding. National Natural Science Foundation of China (61675068, 61675227, 61975016); National Key Research and Development Program of China (2017YFA0303800); Natural Science Foundation of Beijing Municipality (Z190006).

Disclosures. The authors declare no conflicts of interest.

†These authors contributed equally to this work.

REFERENCES

1. N. Yu, P. Genevet, M. A. Kats, F. Aieta, J.-P. Etienne, F. Capasso, and Z. Gaburro, "Light propagation with phase discontinuities: generalized laws of reflection and refraction," Science **334**, 333–337 (2011).

2. A. V. Kildishev, A. Boltasseva, and V. M. Shalaev, "Planar photonics with metasurfaces," Science **339**, 1232009 (2013).
3. N. Yu and F. Capasso, "Flat optics with designer metasurfaces," Nat. Mater. **13**, 139–150 (2014).
4. L. Zhang, S. Mei, K. Huang, and C.-W. Qiu, "Advances in full control of electromagnetic waves with metasurfaces," Adv. Opt. Mater. **4**, 818–833 (2016).
5. P. Genevet, F. Capasso, F. Aieta, M. Khorasaninejad, and R. Devlin, "Recent advances in planar optics: from plasmonic to dielectric metasurfaces," Optica **4**, 139–152 (2017).
6. H.-H. Hsiao, C. H. Chu, and D. P. Tsai, "Fundamentals and applications of metasurfaces," Small Meth. **1**, 1600064 (2017).
7. F. Aieta, P. Genevet, M. A. Kats, N. Yu, R. Blanchard, Z. Gahurro, and F. Capasso, "Aberration-free ultrathin flat lenses and axicons at telecom wavelengths based on plasmonic metasurfaces," Nano Lett. **12**, 4932–4936 (2012).
8. Y.-H. Chen, J.-X. Fu, and Z.-Y. Li, "Surface wave holography on designing subwavelength metallic structures," Opt. Express **19**, 23908–23920 (2011).
9. X. Ni, A. V. Kildishev, and V. M. Shalaev, "Metasurface holograms for visible light," Nat. Commun. **4**, 2807 (2013).
10. W. T. Chen, K.-Y. Yang, C.-M. Wang, Y.-W. Huang, G. Sun, I.-D. Chiang, C. Y. Liao, W.-L. Hsu, H. T. Lin, S. Sun, L. Zhou, A. Q. Liu, and D. P. Tsai, "High-efficiency broadband meta-hologram with polarization-controlled dual images," Nano Lett. **14**, 225–230 (2014).
11. G. Zheng, H. Mühlenbernd, M. Kenney, G. Li, T. Zentgraf, and S. Zhang, "Metasurface holograms reaching 80% efficiency," Nat. Nanotechnol. **10**, 308–312 (2015).
12. Q. He, S. Sun, and L. Zhou, "Tunable/reconfigurable metasurfaces: physics and applications," Research **2019**, 1849272 (2019).
13. A. Nemati, Q. Wang, M. Hong, and J. Teng, "Tunable and reconfigurable metasurfaces and metadevices," Opto-Electron. Adv. **1**, 180009 (2018).
14. Y. Yao, R. Shankar, M. A. Kats, Y. Song, J. Kong, M. Loncar, and F. Capasso, "Electrically tunable metasurface perfect absorbers for ultrathin mid-infrared optical modulators," Nano Lett. **14**, 6526–6532 (2014).
15. Y.-W. Huang, H. W. H. Lee, R. Sokhoyan, R. A. Pala, K. Thyagarajan, S. Han, D. P. Tsai, and H. A. Atwater, "Gate-tunable conducting oxide metasurfaces," Nano Lett. **16**, 5319–5325 (2016).
16. L. Liu, L. Kang, T. S. Mayer, and D. H. Werner, "Hybrid metamaterials for electrically triggered multifunctional control," Nat. Commun. **7**, 13236 (2016).
17. B. Gholipour, J. Zhang, K. F. MacDonald, D. W. Hewak, and N. I. Zheludev, "An all-optical, non-volatile, bidirectional, phase-change meta-switch," Adv. Mater. **25**, 3050–3054 (2013).
18. X. Yin, T. Steinle, L. Huang, T. Taubner, M. Wuttig, T. Zentgraf, and H. Giessen, "Beam switching and bifocal zoom lensing using active plasmonic metasurfaces," Light Sci. Appl. **6**, e17016 (2017).
19. J. Y. Ou, E. Plum, J. F. Zhang, and N. I. Zheludev, "An electromechanically reconfigurable plasmonic metamaterial operating in the near-infrared," Nat. Nanotechnol. **8**, 252–255 (2013).
20. M. L. Tseng, J. Yang, M. Semmlinger, C. Zhang, P. Nordlander, and N. J. Halas, "Two-dimensional active tuning of an aluminum plasmonic array for full-spectrum response," Nano Lett. **17**, 6034–6039 (2017).
21. A. She, S. Zhang, S. Shian, D. R. Clarke, and F. Capasso, "Adaptive metalenses with simultaneous electrical control of focal length, astigmatism, and shift," Sci. Adv. **4**, eaap9957 (2018).
22. S. Sun, W. Yang, C. Zhang, J. Jing, Y. Gao, X. Yu, Q. Song, and S. Xiao, "Real-time tunable colors from microfluidic reconfigurable all-dielectric metasurfaces," ACS Nano **12**, 2151–2159 (2018).
23. E. Arbabi, A. Arbabi, S. M. Kamali, Y. Horie, M. Faraji-Dana, and A. Faraon, "MEMS-tunable dielectric metasurface lens," Nat. Commun. **9**, 812 (2018).
24. T. Roy, S. Zhang, I. W. Jung, M. Troccoli, F. Capasso, and D. Lopez, "Dynamic metasurface lens based on MEMS technology," APL Photon. **3**, 021302 (2018).
25. S.-Q. Li, X. Xu, M. V. Rasna, V. Valuckas, R. Paniagua-Domínguez, and A. I. Kuznetsov, "Phase-only transmissive spatial light modulator based on tunable dielectric metasurface," Science **364**, 1087–1090 (2019).
26. T. Kan, A. Isozaki, N. Kanda, N. Nemoto, K. Konishi, H. Takahashi, M. Kuwata-Gonokami, K. Matsumoto, and I. Shimoyama, "Enantiomeric switching of chiral metamaterial for terahertz polarization modulation employing vertically deformable MEMS spirals," Nat. Commun. **6**, 8422 (2015).
27. Z. Liu, H. Du, J. Li, L. Lu, Z.-Y. Li, and N. X. Fang, "Nano-kirigami with giant optical chirality," Sci. Adv. **4**, eaat4436 (2018).
28. J. Li and Z. Liu, "Focused-ion-beam-based nano-kirigami: from art to photonics," Nanophotonics **7**, 1637–1650 (2018).